Pergamon

Available online at www.sciencedirect.com
SCIENCE DIRECT®

Cement and Concrete Research 33 (2003) 1347–1355

CEMENT AND CONCRETE RESEARCH

Thermal and hygric properties of Portland cement mortar after high-temperature exposure combined with compressive stress

R. Černý[a,*], M. Totová[a], J. Poděbradská[a], J. Toman[b], J. Drchalová[b], P. Rovnaníková[c]

[a]*Department of Structural Mechanics, Faculty of Civil Engineering, Czech Technical University, Thákurova 7, Dejvice 16629, Prague 6, Czech Republic*
[b]*Department of Physics, Faculty of Civil Engineering, Czech Technical University, Thákurova 7, Prague 6 16629, Czech Republic*
[c]*Institute of Chemistry, Faculty of Civil Engineering, Technical University of Brno, Zižkova 17, Brno 66237, Czech Republic*

Received 2 March 2001; accepted 11 February 2003

Abstract

Thermal conductivity λ, water vapor permeability δ, and liquid moisture diffusivity κ of cement mortar are measured on specimens subjected to four types of pretreatment, namely, unloaded, mechanically loaded to 90% of compressive strength, thermally loaded by subjecting to a temperature of 800 °C for 2 h, and loaded both mechanically and thermally. The values of λ and κ are found to depend very significantly on the loading mode. The maximum differences observed compared to the unloaded samples are almost one order of magnitude for λ and as much as three orders of magnitude for κ. In contrast, the values of δ are found to increase by only about 40% compared to the basic unloaded material. It is proposed that the observed large differences in λ and κ are due to the formation of cracks and the increase of total pore volume, which were shown by visual analysis and mercury porosimetry.

Keywords: Transport properties; Hygric properties; Mercury porosimetry; Thermal analysis

1. Introduction

Standard lists of thermal and hygric properties of building materials usually include constant values only, regardless of any influence of external parameters (see Ref. [1] for an extensive analysis of thermal and hygric "calculation" values in six European standards B, NL, F, FRG, I, and UK). Some of the parameters are given at least in some standards in a more precise way; for instance, in Ref. [2], the thermal conductivity is assumed as a function of moisture content. However, some of the parameters commonly used in practice are missing in most of the standards (e.g., the liquid moisture transport parameters and the moisture storage parameters).

Therefore, in building physics or fire protection-related calculations, the lists of "calculation" values given in standards can be effectively employed in preliminary or simplified overall analyses only. Also, in standard conditions, where, for instance, temperature and moisture are in well-defined and not very extended limits, the standard lists of data can be used without any significant loss of accuracy. However, in nonstandard conditions, such as the high-temperature exposure of a material, a more fundamental approach is desirable, which may require not only the "calculation" values but also their relationships to the important influencing parameters.

For concrete, cement mortars, and cement pastes, the situation is not any better than for other building materials. Basic parameters can be found in the cited general standards for building materials. Other sources for typical values of thermal and hygric parameters are standard textbooks on the properties of concrete, such as the well-known book by Neville [3]. If more comprehensive data on some specific thermal or hygric parameter are required, one has to look for it in specialized journals and/or specialized books.

A comprehensive survey of the thermal properties of concrete, cement mortar, and cement paste at high temperatures can be found in the book by Bažant and Kaplan [4]. The influence of crack formation on the water permeability of concrete was measured by Bažant et al. [5], Wang et al. [6], and Aldea et al. [7]. Diffusion properties of cracked

* Corresponding author. Tel.: +420-2-2435-4429; fax: +420-2-2431-0775.
E-mail address: cernyr@fsv.cvut.cz (R. Černý).

0008-8846/03/$ – see front matter © 2003 Elsevier Science Ltd. All rights reserved.
doi:10.1016/S0008-8846(03)00067-X

concrete were studied by Gerard and Marchand [8]. Temperature and moisture dependence of wood–cement composite were analyzed by Bouguerra [9]. Černý et al. [10] investigated the effect of compressive stress on the thermal and hygric properties of Portland cement mortar in wide temperature and moisture ranges.

The work presented in this paper goes beyond the scope of measurements, which were done in Ref. [10], and analyzes thermal conductivity, water vapor permeability, and liquid moisture diffusivity of cement mortar for four sample conditions, namely, unloaded, mechanically loaded to 90% of compressive strength, thermally loaded by exposure at 800 °C for 2 h, and loaded both mechanically and thermally.

2. Materials and samples

The measurements of thermal and hygric parameters were done on the samples of cement mortar with the following composition (i.e., the mixture for one charge): Portland cement ENV197-1 CEMI 42.5 R (Kraluv Dvur, CZ)—450 g; natural quartz sand with continuous granulometry I, II, and III (the total screen residue on 1.6 mm is 2%, on 1.0 mm is 35%, on 0.50 mm is 66%, on 0.16 mm is 85%, and on 0.08 mm is 99.3%)—1350 g; and water—225 g. For the sake of data comparison, this composition was exactly the same as in a previous paper [10]. Also, the method of curing in the initial 28-day period was the same. There was only one principal difference in the measuring conditions in Ref. [10]. While in Ref. [10] the loading and measurements were done just after the 28-day curing period, in this work, both loading and measurements were performed with an 8-month delay period after the 28-day curing period. During this delay period, the samples were stored under normal laboratory conditions, at a temperature of 25 °C and a relative humidity of 35%.

The dimensions of the samples were $40 \times 40 \times 120$ mm for room temperature thermal conductivity measurements, and $71 \times 71 \times 71$ mm for high-temperature thermal conductivity measurements. The samples for determining moisture diffusivity and water vapor permeability were cylindrical, with a diameter of 105 mm and a height of 20 mm.

In the experimental measurements, four different cement mortar specimen conditions were analyzed: (1) specimen at room temperature not exposed to any load (denoted by NL); (2) specimen exposed to a gradual temperature increase up to 800 °C during 2 h and then left for another 2 h at 800 °C but without previous mechanical load (TL); (3) specimen exposed to mechanical load of 90% of compressive strength but without thermal load (ML); and (4) specimen exposed first to mechanical load of 90% of compressive strength, then to a gradual temperature increase up to 800 °C during 2 h and finally left for another 2 h at 800 °C (MTL). Three specimens were tested for each pretreatment condition.

3. Measuring methods

3.1. Thermal conductivity

Thermal conductivity λ at room temperature was measured by an ISOMET 2104 device (Applied Precision). ISOMET 2104 is a portable device for direct measurement of thermophysical properties of a wide range of materials. It is equipped with various types of optional probes. Needle probes are suitable for porous, fibrous, or soft materials, and surface cylindrical probes for hard materials. Cylindrical surface probes were employed for the measurements in this work. ISOMET 2104 is based on a dynamic impulse technique, which enables the reduction of the period of thermal conductivity measurement to about 10 min. A built-in menu system on the display enables interactive communication with the device and recalibration of measurement probes using reference materials. Calibration data in the internal memory ensure interchangeability of probes without affecting the measurement accuracy. Measured data are stored in the internal memory and can be transferred into a PC by serial interface RS 232.

For high-temperature measurements, a double integration method was used based on the analysis of the temperature field (see Ref. [11] for details and Ref. [10] for a short overview). The basic principle of this method consists of measuring the temperature field in the sample during one-sided heating, and of the subsequent solution of the inverse heat conduction problem. Using this method, the specific heat and the density of the material as functions of temperature must be known. For the measurements of specific heat at high temperatures, a nonadiabatic method described by Toman and Černý [12] was employed, and the density was determined using thermogravimetric measurements.

The procedure used for $\lambda(T)$ function determination is as follows. One-side heating of a specimen (for concrete or cement mortar typically $71 \times 71 \times 71$ mm) with thermally insulated lateral faces is achieved using a furnace, where a constant temperature is maintained. A set of temperature sensors is positioned along the longitudinal axis of the sample, which makes it possible to record the temperature field through a measuring unit by a PC. From the measured $T(x,t_i)$ curves, a set of 8–10 curves is chosen, and these curves are used in the computational treatment. First, the measured $T(x,t_i)$ curves are subjected to a regression analysis. When a temperature τ_i is chosen, the integration area is determined for this value and the corresponding value of thermal conductivity $\lambda(\tau_i)$ is calculated. This procedure is repeated for a sufficient number of τ_i values, so that a pointwise given function $[\tau_i,\lambda(\tau_i)]$ is finally obtained.

3.2. Hygric parameters

While the material parameters describing heat transfer in porous materials are quite unified, there are a variety of transport coefficients describing moisture transport, which

are commonly used in the practice. This is a consequence of the fact that in the phenomenological relations, applied in commonly employed models (e.g., see Refs. [13–17]), there appears a variety of generalized thermodynamic forces, including the water partial density gradient, the capillary pressure gradient, the piezometric head gradient, the temperature gradient, the partial density of water vapor gradient, and the partial pressure of water vapor gradient. The corresponding phenomenological coefficients as proportionality factors between the fluxes and forces are, respectively, moisture diffusivity, hydraulic conductivity, water permeability, thermodiffusion coefficient, water vapor diffusion coefficient, and water vapor diffusion permeability. The thermodynamic forces are always gradients of state variables, and not all state variables used in various models are independent. Consequently, algebraic relations can be formulated between some phenomenological parameters.

Generally, all models employed in practical calculations work with at least two forces and two respective phenomenological coefficients called hygric parameters—one of them for water and the second one for water vapor. In this paper, the hygric parameters employed in the model by Häupl and Stopp [15] are used, namely, the moisture diffusivity κ and the water vapor permeability δ, defined in the following way:

$$j_v = -\delta \operatorname{grad} p_v, \tag{1}$$

$$j_w = -\kappa \operatorname{grad} \rho_m, \tag{2}$$

where j_v is the flux of water vapor, p_v is the partial pressure of water vapor, j_w is the water flux, and ρ_m is the mass of water per unit volume of the porous body (partial density of water or moisture density in the sense of the classical linear theory of mixtures).

For the determination of moisture diffusivity κ, a simple method was employed based on the assumption that κ can be considered as piecewise constant with respect to the moisture density ρ_m (i.e., the PCK method; see Ref. [18] for details and Ref. [10] for a short overview). In contrast to the most frequently used methods for κ determination such as the Matano method [19], the PCK method is very fast even for materials with low κ; in addition, it exhibits reasonable precision (see Ref. [20] for a more detailed analysis). Therefore, its application for cement mortar is very suitable.

The experimental set-up of the PCK method is identical with that of a common water sorption experiment (e.g., see Ref. [21]). The specimens having the form of a plate or a prism are water- and vapor-proof insulated on all lateral sides (i.e., the sides parallel to the main direction of water transport) using, for example, an epoxy resin. The specimens are then located in such a manner that the lower surface is placed in contact with water. This can be achieved by suspending the specimens above a water reservoir or putting them on a sponge, allowing them to suck water from a free water surface. The mass of the specimen is recorded as a function of time, either automatically or in the simplest case, just by interrupting the experiment at the chosen time intervals and weighing the specimen. In this way, the amount of water in the specimen as a function of time is determined. Assuming κ to be constant over a certain (not very wide) range of moisture contents, an analytical solution of the moisture transport equation can be employed to determine κ, which is the only unknown parameter.

In practice, measurements are usually made on a set of specimens with various values of initial partial moisture density, and the corresponding set of values of moisture diffusivity $\kappa(\rho_{m,c})$ is determined (see Ref. [18]). In this way, a relationship can be obtained between moisture diffusivity and partial moisture density.

In this work, only one characteristic value of moisture diffusivity was determined for every group of specimens because the primary aim was to obtain a comparison of the effects of mechanical and thermal loads on moisture transport. As the initial state of specimens was dry material, the measured values of κ correspond to approximately one half of the water saturation value (see Ref. [18]).

The measuring method for the determination of the water vapor permeability δ is described in detail in Ref. [22]. The experiment is carried out under isothermal conditions. The measuring device consists of two airtight glass chambers separated by a plate-type specimen of the measured material. In the first chamber, a state near 100% relative humidity is maintained (by incorporating an open container filled with water in the chamber), while in the second one, there is a state close to 0% relative humidity (achieved by incorporating silica gel in the chamber). The changes in the mass of water in the container (Δm_w) and of the silica gel (Δm_a) are recorded at appropriate time intervals. The method is transient so that only a few hours are necessary to obtain results for water vapor transmission properties. However, steady-state measurements can also be done. In that case, the validity of the condition $|\Delta m_w| = |\Delta m_a|$ is tested and the experiment continues until this condition is realized.

Compared to the classical cup method, employed in European and American standards (Refs. [23,24]), this experimental set-up has the advantage that constant relative humidity needs to be maintained only in a relatively small chamber, and the flux of water vapor across the specimen is measured. As a consequence, not only the transient experiments (which is quite obvious) but also the steady-state measurements are significantly faster than in the classical cup method set-up.

For the determination of δ, Dirichlet boundary conditions (i.e., constant partial water vapor pressure equal to that in the particular chamber) are assumed, and constant initial conditions are established. Then, for δ = constant, an analytical solution can be found. Using this analytical solution, the incoming and outcoming fluxes of water vapor can be calculated. As these fluxes are known from the measure-

ments, δ remains the only unknown in the final equation (see Ref. [22] for details):

$$m_w(\tau)+\frac{2Sd}{\pi^2}\left[-\frac{M}{R}T^{C-1}\times 10^{-\frac{A}{T}+B}\sum_{n=1}^{\infty}\frac{1}{n^2}(\varphi_o-\varphi_d\cos(n\pi))\times\left(1-\exp\left(-\frac{Dn^2\pi^2\tau}{d^2}\right)\right)+\rho_{co}\sum_{n=1}^{\infty}\frac{1}{n^2}\times\left(1-\exp\left(-\frac{Dn^2\pi^2\tau}{d^2}\right)\right)(1-\cos(n\pi))\right]-\frac{SD}{d}\frac{M}{R}(\varphi_o-\varphi_d)T^{C-1}\times 10^{-\frac{A}{T}+B}\tau=0, \quad (3)$$

where m_w is the mass of water that penetrated into the specimen during the time interval τ; φ_o and φ_d are the relative humidities in the wet and dry chamber, respectively; d is the thickness of the specimen, S is the surface area of the specimen in contact with the prescribed environment in the chamber; T is the temperature in degrees Kelvin; R is the universal gas constant; M is the molar mass of water vapor; D is the diffusion coefficient of water vapor in the porous material [where $D=\delta\{(RT)/M\}$]; and A, B, and C are empirical constants ($A=2900$ K; $B=24.738$; and $C=-4.65$).

4. Experimental results

4.1. Thermal conductivity

The thermal conductivity of the four groups of specimens exposed to four mechanical and thermal pretreatment conditions, as described in Section 2, was first determined at room temperature using the ISOMET 2104 device. Then, the high-temperature measurements were done using the one-side heating and double integration method. The initial state of the specimens for measurement was always the dry state.

The results of room temperature measurements are summarized in Table 1, where each value is the average of 10 measurements. The mechanical loading had only a small effect on the value of thermal conductivity, and the differences were of the order of the error range limit of the measuring method. In contrast, the influence of thermal load was very substantial and resulted in a decrease of thermal conductivity to about one quarter of the reference value. The combination of thermal and mechanical loads resulted in only slightly higher values of thermal conductivity than in the case of thermal load only, which can be considered to be again on the edge of the error range.

Table 1
Thermal conductivity of cement mortar in room temperature conditions

Sample	λ (W/mK)
NL	1.16
ML	1.05
TL	0.27
MTL	0.35

The results of high-temperature measurements are given in Fig. 1. In this case, the TL samples achieved the highest λ values, the MTL samples exhibited λ values 10–30% lower than these, and the lowest values were exhibited by the NL and ML samples. According to the analysis, reported in Ref. [11], the overall accuracy of the determination of the thermal conductivity using the double integration method is about ±15%. Therefore, it can be assumed that the differences between the groups (i.e., TL, MTL, NL, and ML) are outside the error range of the measurements.

4.2. Hygric parameters

The experimental results of measurements of hygric parameters are summarized in Table 2. Apparently, the influences of thermal and mechanical loads were more pronounced for moisture diffusivity κ than for water vapor permeability δ. While the values of δ increased by a maximum of only 40% (i.e., for MTL) compared to the reference unloaded specimens, the values of κ increased up to three orders of magnitude.

The effect of mechanical load was significant for κ only, where it has led to an increase of about one order of magnitude, and the differences in δ between NL and ML were within the error range of the experimental method. The thermal load resulted in an increase of κ of about three orders of magnitude but only a 20% increase of δ. The combination of thermal and mechanical loads has led to an increase of κ of about two orders of magnitude and a 40% increase of δ.

4.3. Characterization experiments

In order to analyze the reasons for the observed changes in thermal and hygric parameters after thermal and mechanical loadings, characterization experiments were done, namely, visual analysis, mercury porosimetry (MP), and differential thermal analysis (DTA) were used.

The visual analysis as the simplest method for the damage assessment of the different sample categories revealed an appearance of wide cracks for TL and MTL samples, but not any visible cracks for ML samples. The cracks were distributed in a random way and differed for different samples of the same category. Therefore, no conclusions concerning the crack width and crack distance could be made.

Porosimetric measurements were performed using the mercury porosimeter AutoPore 2000 (Micromeritics) on the four categories of specimen: NL, ML, MTL, and TL. The results are shown in Table 3, which presents a summary

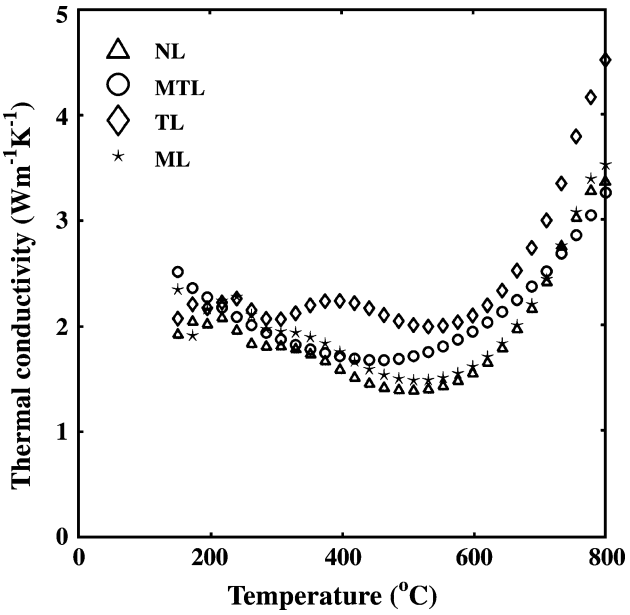

Fig. 1. High-temperature values of the thermal conductivity of cement mortar for various types of previous loadings.

of the global characteristics of the particular specimens: V_p is the total intrusion volume, A_p is the total pore area, r_v is the median pore radius by volume, and ρ is the bulk density of the material. Apparently, when mechanical load was applied, only minor changes in global parameters appeared; for instance, V_p increased only by 8% and r_v by 21% compared to the reference specimen NL. On the other hand, thermal load resulted in much more pronounced effects. The median pore radius increased by about 15 times compared to the reference specimen NL, V_p increased by almost 70%, and even ρ decreased by 8%. The combination of mechanical and thermal loads (MTL) has led to very similar results as in the case when only thermal load (TL) was applied; V_p and ρ were almost the same (i.e., within the error range of experimental measurements). However, the median pore radius for MTL decreased by two and a half times compared to TL and the total pore area increased by almost two times.

Thermal analysis was carried out using the equipment SETARAM TG DTA Analyzer 92-10. The samples were heated to a temperature of 1200 °C, and the mass of the particular samples was 40 mg. The results of DTA and TG measurements are shown in Figs. 2 and 3.

Fig. 2 shows DTA curves of NL and TL samples. On the curve corresponding to NL sample, the first very pronounced endothermic peak (a minimum) at 107 °C is clearly the evaporation of pore water. This peak probably also includes the decomposition of CSH gels that should take place between 120 and 140 °C (Ref. [25], p. 201) and the decomposition of ettringite around 120 °C (see Ref. [25], p. 177). The second endothermic peak at 212 °C corresponds to the decomposition of the aluminate phase $4CaO{\cdot}Al_2O_3{\cdot}13H_2O$ and sulfoaluminate phases $3CaO{\cdot}Al_2O_3{\cdot}CaSO_4{\cdot}12H_2O$ and $3CaO{\cdot}Al_2O_3{\cdot}3CaSO_4{\cdot}31H_2O$ (see Ref. [25], pp. 176–177). The third significant endothermic peak at 460 °C represents the decomposition of $Ca(OH)_2$ (Ref. [25], p. 207):

$$Ca(OH)_2 \rightarrow CaO + H_2O.$$

The sharp endothermic peak at 573 °C is apparently not related to the processes in cement. It shows the $\beta \rightarrow \alpha$ phase transition of aggregate SiO_2. The wide endothermic peak with a minimum at 710 °C can be assigned to the decomposition of calcium carbonate:

$$CaCO_3 \rightarrow CaO + CO_2,$$

which appeared in the material due to the carbonation of calcium hydroxide. The other small peaks in the range of 800–1200 °C on the DTA curve of the NL sample in Fig. 2 are difficult to identify because their explanation is not reported—as far as the authors know—in the literature.

Table 2
Hygric parameters of cement mortar

Sample	κ (m^2/s^{-1})	δ (s)
NL	9.7×10^{-9}	3.34×10^{-12}
ML	9.0×10^{-8}	3.18×10^{-12}
TL	1.0×10^{-5}	4.03×10^{-12}
MTL	1.3×10^{-6}	4.56×10^{-12}

Table 3
Global characteristics of the pore space of cement mortar

Specimen	V_p (cm^3/g)	A_p (m^2/g)	r_v (μm)	ρ (kg/m^3)
NL	0.073	13.62	0.038	2200
TL	0.122	5.46	0.565	2020
ML	0.079	11.26	0.046	2150
MTL	0.127	9.49	0.219	1980

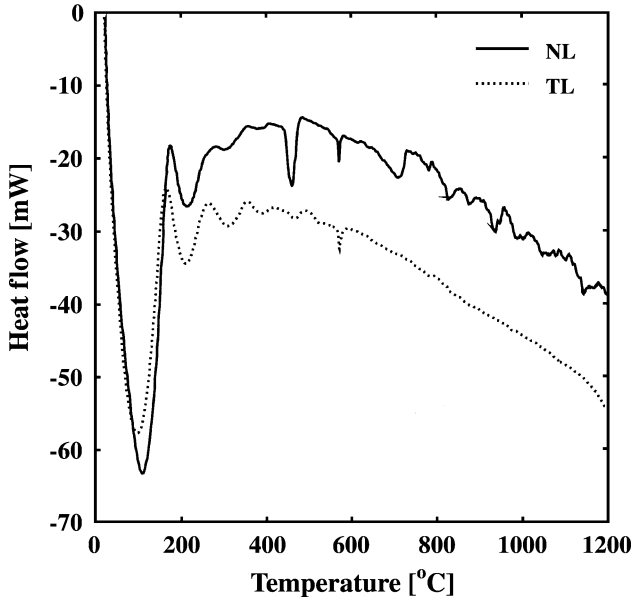

Fig. 2. DTA curves of cement mortar.

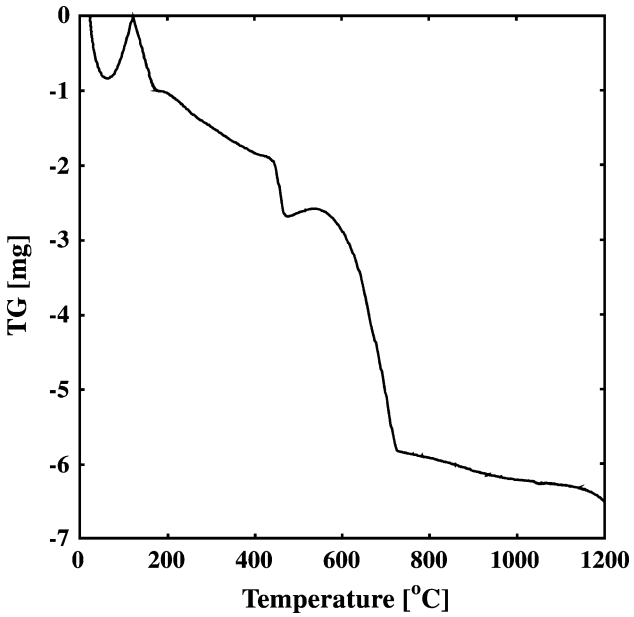

Fig. 3. The TG curve of cement mortar (NL specimen).

The DTA curve of the TL sample in Fig. 2 shows that the two peaks most important for the mass loss at 460 and 710 °C, which were observed on the NL sample curve, are missing. This is due to complete decomposition of $Ca(OH)_2$ and $CaCO_3$ when the samples are thermally loaded.

Fig. 3 shows the TG curve of the NL sample (the curve for the TL sample is not included because the mass loss was too low—out of the scale for the NL sample). It should be noted first that the two periods of mass increase at temperatures of 125 and 540 °C cannot be explained logically because there is—as far as the authors know—no chemical reaction that could explain them. Most probably, this increase is due to a measuring error.

The total mass loss observed was 16.25%. The first remarkable mass loss below 200 °C is approximately 1 mg (i.e., 2.5% of the mass of the sample) and corresponds to the loss of nearly free water from the pore space and water released from CSH gels and ettringite. Further slower mass decreases on the TG curve up to approximately 400 °C can be attributed to the decomposition of aluminate and sulfoaluminate phases. It amounts to 0.93 mg (2.33% of mass) and corresponds to the loss of water from these phases. The fast mass decrease between 450 and 470 °C is due to the decomposition of calcium hydroxide. The amount of water released during this decomposition was 0.786 mg (1.97% of mass), which corresponds to 3.23 mg of $Ca(OH)_2$ in the sample (i.e., 8.07%). The remarkable mass loss between 600 and 710 °C (3.13 mg; i.e., 7.83% of mass) can be assigned to the decomposition of calcium carbonate. The amount of released CO_2 corresponds to 5.26 mg of originally present $CaCO_3$. The slow mass loss at temperatures higher than 710 °C is not discussed in the literature available to the authors.

5. Discussion

As shown by the DTA and TG experiments, the primary reasons for the observed changes in hygric and thermal properties were two chemical reactions affecting the cement binder in the high-temperature range, namely, the decomposition of $Ca(OH)_2$ at 460 °C and the decomposition of $CaCO_3$ at 710 °C. However, the magnitude of these changes was found to depend on the mode of loading of the specimens before the measurements.

In the analysis of the nature of changes of material properties due to the different modes of loading, it seems reasonable to begin with the parameter that was affected in the most significant way (i.e., the moisture diffusivity κ).

Theoretically, the large differences in κ between the thermally loaded samples TL and the reference specimens NL could have both physical and chemical origins. The method for determination of κ employed in this paper is based on the measurement of the total amount of water penetrated into the sample during a specified time. A part of this water could possibly react with some components that appeared in the sample after thermal load. Due to the decomposition of $Ca(OH)_2$ and $CaCO_3$ evidenced by DTA and TG, the TL samples (and MTL samples as well) should contain a relatively high amount of quicklime. According to the TG analysis mentioned above, there should be 2.44 mg of CaO originating from the decomposition of $Ca(OH)_2$ and 3.98 mg of CaO from the decomposition of $CaCO_3$ (i.e., total of 16.05% of mass). This CaO could be subjected to hydration after getting into contact with the penetrating water in the water uptake experiment for the determination of κ. The theoretical amount of penetrating water that could be immobilized by this reaction and prevented from further transport is 5.15% of mass of the sample, which is quite high.

It is very difficult to make a theoretical estimate of the real amount of water that reacted with quicklime in our particular case. First, the exact amount of CaO in the TL samples is not known because a part of it could be lost during the manual operation of the samples. Also, there was certainly a competition between the rate of chemical reaction and the fast water penetration into the sample. The characteristic time of water uptake in the experiment was, for TL samples, about 10 s. Quicklime itself reacts with water very fast and an explosive nucleation-controlled reaction takes place in direct contact with water, so that in the beginning, this process would certainly be faster than water penetration driven by capillary forces. However, once a new $Ca(OH)_2$ is formed, the reaction becomes diffusion-controlled and slows down in a significant way due to the insufficient amount of water available, and capillary water transport begins to dominate in the process of water interaction with the material.

Therefore, a simple experiment that was intended to show the real effect of quicklime on the values of moisture diffusivity was carried out. This was done, in parallel to

water uptake experiments, with two samples. One of them was the TL sample as described before. The second sample (denoted as TL-S) was first subjected to the same thermal load as the TL sample but, after cooling, it was saturated by capillary water. After achieving the water saturation state, the TL-S sample was left under water for 7 days to ensure that all the CaO present reacted with water and formed $Ca(OH)_2$. Then, both the TL and TL-S samples were dried at 105 °C to a constant mass and, finally, the water uptake experiments were performed, as described in Section 3.2. The results show that the moisture diffusivity of the TL-S sample was 10% lower than the TL sample. This does indicate that the hydration of CaO does influence moisture diffusivity, although it should be noted that the accuracy of the determination of κ by the PCK method is approximately 10%. However, the effect of CaO, if any, is very low, and most probably the major part of quicklime was lost during the manual operation of the samples.

Concentrating now on the physical effects, a comparison of the results of moisture diffusivity measurements for ML and TL specimens shows that the obtained results correlate well in the qualitative sense with the global characteristics of the pore space (see Table 3), so that a higher pore volume leads to a higher value of κ. However, a similarly good correlation was not achieved for MTL specimens where κ was one order of magnitude lower compared to TL and the pore volume was almost the same. This fact can be explained by the following hypothesis: The most important factor influencing the extent of damage of the pore structure is the possibility of gas removal from the porous system. In this respect, the mechanical load applied before the thermal treatment could lead to certain mechanical damages of the pore structure and to an appearance of microcracks already at room temperature. Therefore, during the subsequent thermal load, the increasing pressure could be more easily spatially compensated, the gas transfer from smaller to larger pores was easier, and the extent of the destruction of the pore system was not so high as for the mechanically undamaged specimens. The width of the preferential paths (cracks) opened for the gas removal was then smaller for MTL specimens than for TL, where the microcrack opening could appear due to an explosive process. These preferential paths significantly affected moisture transfer during the water suction experiments and were the primary reason for the observed differences between the κ values of TL and MTL specimens. The results of MP measurements show that also the internal pore system of TL specimens (wide open cracks cannot be detected by MP due to the small sample size) could be damaged by the overpressure induced by the gas production, more than by MTL, because the median pore radius was about 2.5 times higher. This effect further magnified the difference between moisture diffusivity values of TL and MTL specimens.

The lower magnitude of the changes in δ induced by the thermal load compared to κ can be explained using the rough criterion of Knudsen number K_n (see Ref. [26]). Assuming the median pore radius as the quantity characteristic for the porous space, for NL and ML, there is $K_n \sim 1$; for TL and MTL $K_n \sim 0.1$. $K_n \sim 1$ is a value characteristic of the transition region between the viscous flow and Knudsen diffusion; $K_n \sim 0.1$ is somewhere on the edge of the region, where viscous flow begins. Therefore, the modes of water vapor transfer are not very different when comparing NL and TL (i.e., the two extremes). In the transition region, the decrease of the molecular slip effect with increasing pore radius slows down the increase of the phenomenological coefficients in the flux-vs.-force relation (see Ref. [26]). This could be the main reason for the observed relatively slow increase of δ.

The character of changes of thermal conductivity λ observed for the room-temperature and the high-temperature conditions requires a more detailed analysis. From the basic theory of solid state physics [27], it is known that the Fourier thermal conductivity of crystalline materials decreases with temperature. This can be documented on the properties of a variety of different materials [28]. However, the thermal conductivity of cementitious materials in the high-temperature range cannot be considered in the sense of Fourier heat conduction any longer. The term "apparent thermal conductivity" or "generalized thermal conductivity" seems to be more appropriate in this case (see Ref. [29] for details).

In the transient high-temperature experiments presented in this work, the apparent thermal conductivity λ_{app} includes the effects of the decomposition chemical reactions of cement binder and water evaporation. Both these effects are endothermic so that they consume heat during the thermal conductivity measurement. This should lead to a decrease of measured λ_{app} values. The cement decomposition reactions in the high-temperature range also lead to a substantial increase of total pore volume (Table 3). This should result in the decrease of λ_{app} as well because of the lower thermal conductivity of the air compared to the cement matrix.

However, the increase of the pore volume may be accompanied by the damage of the porous structure. In addition, there may appear wide cracks due to the high-temperature exposure not detected by MP. In the conditions of high temperature gradients induced by one-side heating, this may lead to an intensification of convective heat transfer. The larger dimensions of internal cavities may increase the radiative heat transfer. Both these effects clearly result in a significant increase of the values of λ_{app}.

The effects on the λ_{app} values described above are very difficult to quantify theoretically because heat transfer during the one-side heating experiment is complex, and includes all its basic modes and also the heat sinks. Therefore, an empirical determination of λ_{app} described in this work seems to be a simple and logical solution with a clear relation to practice.

In evaluating the fire resistance of buildings, the time when a wall exposed to a fire from one side is capable of

protecting people on the other side from higher temperatures is considered as an important criterion. The apparent thermal conductivity vs. temperature function measured at a one-side heating experiment in high-temperature conditions makes it possible to calculate this time simply by using this function instead of the Fourier thermal conductivity in common heat conduction computer codes. This makes the work of a designer easier.

The fire-protecting walls are mostly load-bearing structures. Therefore, they are mechanically loaded during their possible fire exposure, and it is useful to know the effect of mechanical load on their thermal conductivity in the high-temperature range. Also, the structures exposed to a fire are often reconstructed and, in their continuing service life after this fire, they may be theoretically exposed to another fire, although this certainly is not an often case. For such structures, knowledge of high-temperature thermal conductivity after thermal load is a necessary condition for the evaluation of their fire protection ability.

In the high-temperature thermal conductivity measurement in this work (Fig. 1), the effect of wide cracks due to the thermal load was clearly the prevailing mechanism affecting λ_{app} in the high-temperature range, so that high-temperature λ_{app} values increased. In the room temperature thermal conductivity measurement, the temperature gradients were local and very low, characteristic of impulse techniques. Therefore, the influence of heat convection and radiation on the thermal conductivity values was minimized, and the increase of the total pore volume after thermal load was the dominating factor for the measured λ values.

In Ref. [10] λ, κ, and δ values of NL and ML specimens were measured after 28 days of curing. A comparison of the data obtained in this work with those in Ref. [10] shows that the values of λ in high-temperature ranges measured in this paper were higher than those in Ref. [10], λ values at room temperature were lower, κ values were higher, and δ values were comparable or slightly lower. These differences can be explained by the approximately 10% higher total pore volume measured in this work compared to Ref. [10]. The probable reason of these changes is the natural aging of the material.

6. Conclusions

Both the mechanical load of 90% of the compressive strength and the thermal load of 800 °C exposure for 2 h, and their combination as well, were found to be factors affecting the thermal conductivity in the high-temperature range in a significant way. Two competing mechanisms, namely, the increase of the total pore volume and the intensification of convective and radiative heat transfers, can have a significant influence on the value of apparent thermal conductivity. In the measurements in this work, the enhanced convective and radiative heat transfers were found to be more important. In contrast, in room temperature conditions, the effect of pore volume increase after mechanical and thermal loadings was found to be dominant, so that a decrease of thermal conductivity after loading was always observed.

The thermal and mechanical loads exhibited a significant influence also on the values of moisture diffusivity κ. The characterization experiments using MP, together with the visual observations, revealed that the main reason for the observed differences in the values of κ for the samples loaded in different ways was the appearance of cracks. Contrary to κ, the values of water vapor permeability δ were affected in a much smaller extent, in contrast to the fact that water vapor transfer in concrete is much easier than liquid water transfer under normal conditions.

The thermal load employed in the experimental work in this paper can roughly simulate, for instance, the effect of a fire of a concrete structure. The concrete structures that survived a fire exposure can often be further utilized after a proper reconstruction. From this point of view, it should be noted that a significant increase of moisture diffusivity can worsen the thermal properties of the wall due to a faster moisture transport, and it can also lead to an increase of hygric stresses in the structure. This has to be taken into account in a possible reconstruction work.

Acknowledgements

This research has been supported by the Ministry of Education of the Czech Republic, under contract no. MSM 210000004.

References

[1] IEA, Annex XIV: Condensation and Energy, International Energy Agency, Leuven, March 1991.
[2] Czech Standard No. 730540-3, Thermal Protection of Buildings. Calculation Values of Quantities for Design and Verification, Czech Standardization Institute, Prague, 1994.
[3] A.M. Neville, Properties of Concrete, 2nd ed., Pitman, London, 1973.
[4] Z.P. Bažant, M.F. Kaplan, Concrete at High Temperatures: Material Properties and Mathematical Models, Longman, Harlow, 1996.
[5] Z.P. Bažant, S. Sener, J.K. Kim, Effect of cracking on drying permeability and diffusivity of concrete, ACI Mater. J. 84 (1987) 351–357.
[6] K. Wang, D.C. Jansen, S.P. Shah, Permeability study of cracked concrete, Cem. Concr. Res. 27 (1997) 381–393.
[7] C.M. Aldea, S.P. Shah, A. Karr, Permeability of cracked concrete, Mater. Struct. 32 (1999) 370–376.
[8] B. Gerard, J. Marchand, Influence of cracking on the diffusion properties of cement-based materials: Part I. Influence of continuous cracks on the steady-state regime, Cem. Concr. Res. 30 (2000) 37–43.
[9] A. Bouguerra, Temperature and moisture dependence of the thermal conductivity of wood–cement-based composite: experimental and theoretical analysis, J. Phys., D, Appl. Phys. 32 (1999) 2797–2803.
[10] R. Černý, J. Maděra, J. Poděbradská, J. Toman, J. Drchalová, T. Klečka, K. Jurek, P. Rovnaníková, The effect of compressive stress on thermal and hygric properties of Portland cement mortar in wide temperature and moisture ranges, Cem. Concr. Res. 30 (2000) 1267–1276.
[11] R. Černý, J. Toman, Determination of temperature- and moisture-de-

pendent thermal conductivity by solving the inverse problem of heat conduction, in: V.P. de Freitas, V. Abrantes (Eds.), Proceedings of the International Symposium on Moisture Problems in Building Walls, University of Porto, Porto, 1995, pp. 299–308.
[12] J. Toman, R. Černý, High-temperature measurement of the specific heat of building materials, High Temp. High Press. 25 (1993) 643–647.
[13] O. Krischer, Die wissentschaftlichen Grundlagen der Trocknungstechnik, 2nd ed., Springer, Berlin, 1963.
[14] A.V. Lykov, Teplo i massoobmen v processach sushki, Gosenergoizdat, Moskva, 1956.
[15] P. Häupl, H. Stopp, Feuchtetransport in Baustoffen und Bauwerksteilen, Thesis, TU Dresden, 1987.
[16] J.R. Philip, D.A. de Vries, Moisture movement in porous materials under temperature gradients, Trans. Am. Geophys. Union 38 (1957) 222–232.
[17] P.C.D. Milly, Moisture and heat transport in hysteretic, inhomogeneous porous media: a matrix head-based formulation and a numerical model, Water Resour. Res. 18 (1982) 489–498.
[18] R. Černý, J. Drchalová, Measuring the moisture diffusivity of board materials, in: V.P. de Freitas, V. Abrantes (Eds.), Proceedings of the International Symposium on Moisture Problems in Building Walls, University of Porto, Porto, 1995, pp. 147–156.
[19] C. Matano, On the relation between the diffusion coefficient and concentration of solid metals, Jpn. J. Phys. 8 (1933) 109–115.
[20] J. Drchalová, R. Černý, J. Havrda, The effect of anisotropy of building materials on the moisture transfer, Acta Polytech. 40 (2000) 32–35.
[21] B.B. Sabir, S. Wild, M. O'Farrell, A water sorptivity test for mortar and concrete, Mater. Struct. 31 (1998) 568–574.
[22] R. Černý, Š. Hošková, J. Toman, A transient method for measuring the water vapor diffusion in porous building materials, in: V.P. de Freitas, V. Abrantes (Eds.), Proceedings of the International Symposium on Moisture Problems in Building Walls, University of Porto, Porto, 1995, pp. 137–146.
[23] European Standard prEN ISO 12572, Hygrothermal Performance of Building Materials and Products—Determination of Water Vapour Transmission Properties, CEN, Brussels, 2000.
[24] ASTM E96-94, Standard Test Methods for Water Vapour Transmission of Materials, ASTM, Philadelphia, 1994.
[25] H.F.W. Taylor, Cement Chemistry, Academic Press, London, 1992.
[26] M. Kaviany, Principles of Heat Transfer in Porous Media, 2nd ed., Springer, New York, 1995.
[27] C. Kittel, Introduction to Solid State Physics, Wiley, New York, 1976.
[28] D.R. Lide (Ed.), CRC Handbook of Chemistry and Physics, 79th ed., CRC Press, Boca Raton, 1998, pp. 12-193–12-199.
[29] J. Toman, R. Černý, Determination of changes in thermal properties of building materials in the conditions of a fire, Proceedings of the CIB World Building Congress, CIB, Wellington, April 2001, pp. 103–113.